32nd Annual International Conference of the IEEE EMBS
Buenos Aires, Argentina, August 31 - September 4, 2010

Automatic Blood Vessel Localization in Small Field of View Eye Images

Mayank Bansal, Sujit Kuthirummal, Jayan Eledath, Harpreet Sawhney, and Richard Stone

Abstract— **Localizing blood vessels in eye images is a crucial step in the automated and objective diagnosis of eye diseases. Most previous research has focused on extracting the centerlines of vessels in large field of view images. However, for diagnosing diseases of the optic disk region, like glaucoma, small field of view images have to be analyzed. One needs to identify not only the centerlines, but also vessel widths, which vary widely in these images. We present an automatic technique for localizing vessels in small field of view images using multi-scale matched filters. We also estimate local vessel properties – width and orientation – along the length of each vessel. Furthermore, we explicitly account for highlights on thick vessels – central reflexes – which are ignored in many previous works. Qualitative and quantitative results demonstrate the efficacy of our method – e.g. vessel centers are localized with RMS and median errors of 2.11 and 1 pixels, respectively in 700×700 images.**

I. INTRODUCTION

Analyzing the structure and properties of blood vessels in the eye is a crucial step in the diagnosis of eye diseases. To diagnose glaucoma, for instance, clinicians examine blood vessels in the optic disc region (shown in Fig. 1(b)) and evaluate the location and change in their 3D structure and widths over time. This assessment is tedious and subjective. Hence, it is desirable to automate this process and make it more objective. To this end, we propose and demonstrate a technique that automatically localizes blood vessels in the eye and also estimates local vessel properties – width and orientation – along the length of each vessel.

Previous works on detecting vessels include use of matched filters tuned to detect particular intensity structures [2], [6], use of multiscale Gabor filters [8], use of image filter outputs as inputs to classifiers [9], and symmetry and asymmetry analysis in the Fourier domain [11]. In [3], eigen values of the Hessian at every pixel are used to detect ridges in the intensity structure. In [1] and [6], vessels are detected by starting from seed points and tracing along vessels as long as a model for vessel appearance is satisfied. These works have largely focused on extracting the vessel network in large field of view images, like the one in Fig. 1(a). However, for diseases of the optic nerve, like glaucoma, clinicians assess blood vessels in the optic disk (bright elliptical area in Fig. 1(a)), which occupies only a small portion of a conventional fundus image – e.g. 7% of the image in Fig. 1(a). Consequently, small field of view images (e.g. Fig. 1(b)) are used, where vessel widths vary widely – from 3 to 33 pixels in 700×700 images. Most works have not dealt with high resolution, small field of view images, and/or such large variations in vessel widths.

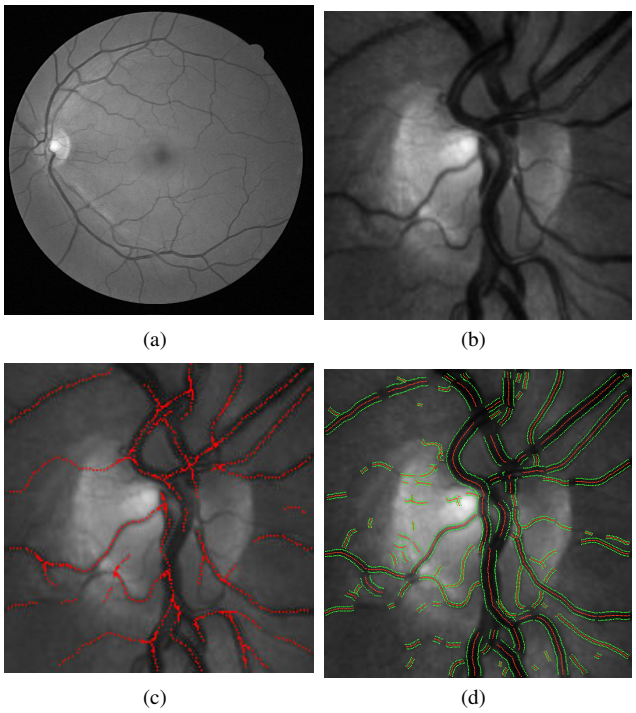

Fig. 1. (a) Large field of view image of the eye. (b) Small field of view image around the optic disc. (c) Vessel centerlines estimated using [9]. (d) Vessel centerlines and boundaries estimated by our proposed approach.

Our approach builds upon the multi-scale matched filter approach of Sofka and Stewart [9]. Their focus is on detecting vessels in large field of view images. Our objective is similar, but the emphasis is different. We aim to accurately localize and characterize vessels: determine vessel centerlines (curves along the center of each vessel) and estimate local vessel properties (width and orientation) at every point on the centerlines. Our focus is on diagnosing diseases like glaucoma that, as noted earlier, requires analyzing small field of view images. Such images have a wide range of vessel widths which makes the problem challenging. In a wide field of view image, like Fig. 1(a) where vessel widths do not vary widely, detection might be equivalent to localization. However, that is not the case for small field of view images like Fig. 1(b). In their work, Sofka and Stewart [9] input responses from matched filters to a learning algorithm to determine which pixels lie on blood vessels and then use

Supported by NEI grant EY-017299, the Mackall Foundation Trust, and Research to Prevent Blindness.

Mayank Bansal, Sujit Kuthirummal, Jayan Eledath and Harpreet Sawhney are with Sarnoff Corporation, Princeton, USA {mbansal, skuthirummal, jeledath, hsawhney}@sarnoff.com

Richard Stone is with the Scheie Eye Institute, University of Pennsylvania, USA stone@mail.med.upenn.edu

non-maximal suppression to generate centerlines. However, accuracy and smoothness of the centerlines was not a goal of their work. Accurate centerlines are necessary for correctly visualizing and comparing blood vessel networks, both in 2D and 3D.

Though our objective is different from Sofka and Stewart [9], for comparison Fig. 1(c) shows the vessel centerlines obtained using their approach. For this result we used code from the authors. However, that implementation was trained on large field of view images with a small range of vessel widths. Therefore, to get reasonable results we had to scale down the image by a factor of 4. This is the reason the centerlines are sparse and appear quantized. Note that their approach misses vessel segments with a central reflex – thick vessel segments with a highlight. We explicitly handle such vessel segments.

To summarize, we make the following contributions:

- We demonstrate a novel algorithm based on multi-scale matched filters and ridge detection that accurately locates centerlines of blood vessels in images which exhibit a wide variation in vessel widths (Sec. II-A and II-B). Fig. 1(d) shows an example where the centerlines are marked in red.
- For each pixel on the centerlines, we also estimate the local properties of the vessel – width and orientation (Sec. II-C). Some diseases like retinopathy of prematurity (ROP) are characterized by significant dilation of vessels and increase in their tortuosity. Quantitative measurement of vessel properties can thus enable automatic and objective diagnosis of such diseases.
- We also account for central reflexes which are ignored in most works (Sec. II-D). If unaccounted for, these result in incorrect estimation of vessel centerlines and local vessel properties, especially in small field of view images.

II. AUTOMATIC VESSEL LOCALIZATION

A. Matched Filter based Vessel Detection

Blood vessels in the eye have a characteristic intensity structure. They are darker than their surroundings. Also, they have a Gaussian like intensity profile across the vessel (normal direction) and are almost uniform along the vessel (tangential direction) [1]. To detect such structures, several works have proposed using matched filters [2], [9]. A matched filter gives a high response when its orientation and shape is similar to the intensity profile. To understand its operation, consider a horizontal vessel with width w. To detect this vessel, we can use a matched filter that is a convolution of two 1D filters – Laplacian of a Gaussian filter in the vertical direction (across the vessel) and a Gaussian filter in the horizontal direction (along the vessel). The first detects Gaussian-like intensity structures, while the second smoothes responses along the vessel. We denote the bandwidths for the two Gaussians as σ_n and σ_t, respectively. We get maximal response for a pixel on the center of the vessel – pixel on the centerline – when $\sigma_n = \lfloor \frac{w}{2} \rfloor$. To detect vessels with different widths, we use filters obtained by varying σ_n; σ_t is kept fixed. To detect vessels with different orientations, we apply the filter at different orientations.

B. Centerline Localization

Given the matched filter responses, at every pixel we pick the maximum response over all scales σ_n to get a single Maximal Response (MR) map. In addition, at each pixel we record the scale and orientation corresponding to the maximum response as the best scale s_i and orientation θ_i. The centerline of a vessel can be identified from the MR map by performing ridge detection [5] at a scale corresponding to the width of that vessel. Ridge detection at other scales would result in incorrect localization of the centerline. Therefore, we perform ridge detection at multiple scales, where the scales correspond to the same range of vessel widths used for computing the MR map[2]. Of the ridges detected at a particular scale, say σ_k, we keep ridges at only those pixels i, whose best scale s_i lies in $[\sigma_k - \mathcal{T}_\sigma, \sigma_k + \mathcal{T}_\sigma]$, where $\mathcal{T}_\sigma$ is typically 3. The selected continuous ridge pixels form the centerline of vessel segments at that scale.

The vessel segments detected at different scales are then combined to get the final vessel network using a technique guided by the intuition that vessel segments detected at the correct scale would be longer than those detected at an incorrect scale. We first sort the vessel segment centerlines detected at all scales in descending order of length. From this list, we add new segments to the final list, if less than 20% of the new segment's pixels overlap with segments already in the final list. The final centerline pixels (xc_i, yc_i) along with the corresponding best scales s_i and orientations θ_i form the set: $(xc_i, yc_i, w_i, \theta_i)$, which represents the localization of the vessel centerlines and the local vessel properties. Here, $w_i = 2 * s_i + 1$.

For all results in the paper we have used the same matched filter parameters: $\sigma_t = 6$ (empirically determined), σ_n is varied from 1 to 16 in increments of 1 (vessel widths can vary from 3 to 33 pixels), and the filter is applied at 36 orientations (every 5°).

C. Smoothing Estimated Vessel Properties

We can use vessel width w_i and orientation θ_i estimated for every centerline pixel (xc_i, yc_i) to trace out pixels on vessel boundaries (xb_i, yb_i):

$$(xb_i, yb_i) = (xc_i, yc_i) \pm \frac{w_i}{2}(\sin\theta_i, \cos\theta_i). \qquad (1)$$

However, as can be seen in Fig. 2(b), individual estimates of width and orientation are noisy, resulting in fragmented vessel boundaries. One approach to refine or smooth these estimates is to perform regression on them, as they are expected to vary smoothly along a vessel. However, it is unclear which global model best describes the variation of these parameters. Hence, we use locally linear regression with a regularizing prior. In particular, we use kernel ridge regression [4].

[1]This is generally the case except for central reflexes on thick vessels. We address such cases in Section II-D.

[2]The scale σ used for ridge detection is $\frac{1}{4}$ of the vessel width being considered.

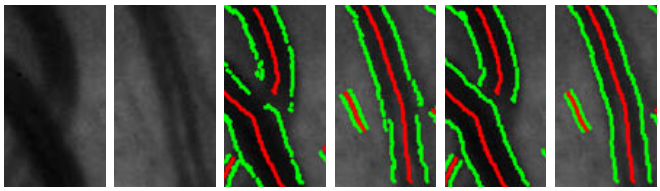

(a) (b) (c)

Fig. 2. (a) Zoomed in portions of an image. (b) Vessel boundaries obtained on using only matched filters (Sections II-A and II-B). (c) Vessel boundaries obtained after regression on the local vessel widths and orientations (Section II-C).

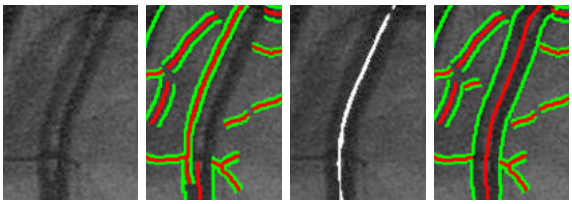

(a) (b) (c) (d)

Fig. 3. (a) Zoomed in portion of vessel with central reflex. (b) Vessels localized without accounting for central reflex. (c) Detected central reflex pixels are shown in white (d) Vessel localized after accounting for central reflex.

For each vessel segment, we perform two independent kernel ridge regressions – one for the estimated widths and the other for the estimated orientations – both as a function of the coordinates of the corresponding centerline pixels. Let u_i denote one of N points in the domain of the regression – coordinates of vessel centerline pixels (x_i, y_i) – and v_i denote the corresponding points in the range – estimated width or orientation. Kernel ridge regression seeks a matrix of regression coefficients W that minimizes the following cost function for a point u in the domain:

$$C(u) = \sum_{i}^{N} |v_i - W^T u_i|^2 k(u, u_i, \sigma) + \frac{W^T W}{2\lambda}, \quad (2)$$

where, $k(u, u_i, \sigma)$ is the Radial Basis Function (RBF) kernel with standard deviation σ and λ controls the influence of the prior – the second term of the equation – which measures the smoothness of the regression fit. As shown in [4], the 'fitted' estimate obtained on minimizing the cost function in Equation 2 is given by

$$\hat{v_i} = \sum_{j}^{N} \alpha_{ij} k(u_i, u_j, \sigma) v_j, \quad (3)$$

where α is the matrix $(K + I/\lambda)^{-1}$, K is the matrix obtained by evaluating the pairwise RBF kernel for all input points in the domain, and I is the identity matrix. The fitted $\hat{v}$ are a weighted linear combination of the inputs v_i, where the weights are determined by the distance between points in the domain.

Fig. 2(c) shows the vessel boundaries obtained on using the widths and orientations obtained after regression, traced out as per Equation 1. As one can see, the vessel boundary contours are smooth and nicely follow the real boundary. For all the results in the paper, we have used the same parameter values for regression: $\lambda = 1$ for both vessel width and orientation regressions, $\sigma^2 = 0.1$ for the width regression, and $\sigma^2 = 0.02$ for the orientation regression. For each regression, the domain (u) and range (v) values were normalized using a scale factor to be in the range $[0, 1]$.

D. Vessels with a Central Reflex

Thick vessels sometimes have highlights in the center called the central reflex. Fig. 3(a) shows one such example. Such vessel regions do not fit the assumption of Gaussian variation of intensity across the vessel as described in Section II-A. Consequently, these are not detected by the matched filter. Most previous works do not account for the effects of the central reflex, since they deal with low resolution, large field of view images. However, in high resolution or small field of view images, central reflex causes errors, as can be seen in Fig. 3(b). In particular, the darker vessel regions on both sides of the reflex get incorrectly detected as one or two separate vessels. Vermeer et al. [10] proposed combining two such incorrect detections into a central reflex vessel detection using some heuristics. Narasimha-Iyer et al.[7] proposed detecting vessels with central reflex by incorporating a generalized dual-Gaussian model for the intensity profile of the vessels into a robust hypothesis testing framework.

In order to be able to correctly detect and localize vessels with a central reflex, we adopt the following workflow. Given the input image, we first detect pixels on central reflexes and then eliminate them by filling-in with intensities interpolated from neighboring pixels. This new filled-in image is then processed by our matched filter based algorithm described in Sections II-A, II-B, and II-C. Though the filling-in does not necessarily produce a Gaussian-like intensity structure across vessels, we have found that the matched filters are able to correctly detect them.

We identify central reflex regions by exploiting their characteristic intensity structure. They typically have an intensity peak in the center, with dark vessel regions around them, which in turn are surrounded by brighter pixels on the retinal surface. That is, the center pixels form a ridge, while the surrounding dark vessel regions form valleys. (See Fig. 3(a)). To detect such intensity structures we perform ridge detection on the intensity image, which gives ridges at the central reflex pixels. To eliminate false detections, on the ridge response image we select only those ridges which have symmetric valleys (darker vessel regions) around them. This structure is localized using the same match filter of Section II-A applied at different scales and orientations. Fig. 3(c) shows the central reflex pixels detected using this approach, while Fig. 3(d) shows the vessel being correctly detected after filling-in the central reflex pixels using cubic interpolation of neighboring intensities.

III. RESULTS

The top row of Fig. 4 shows small field of view images of the optic disk region from 3 different eyes. The results of our technique are shown in the bottom row – the vessel

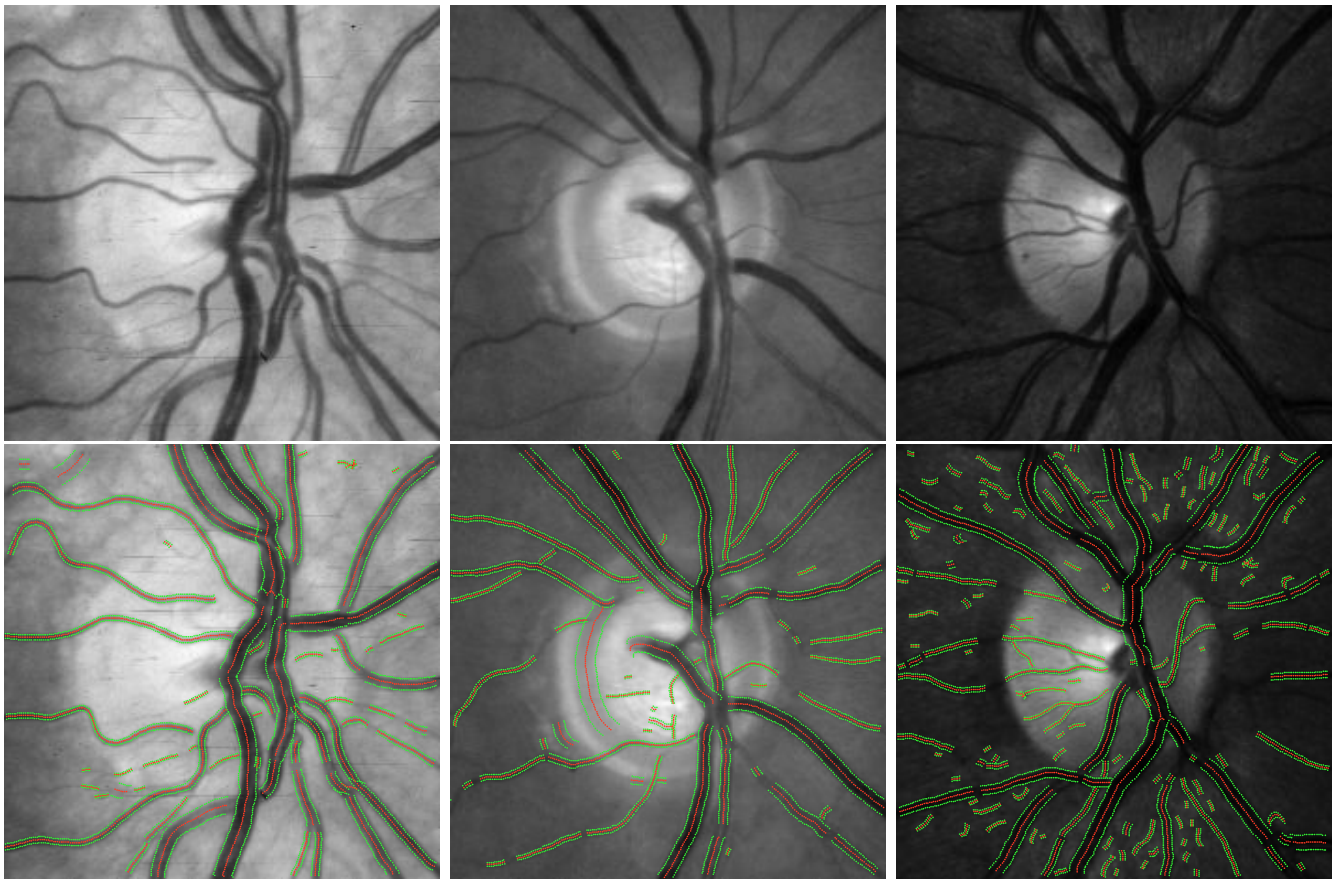

Fig. 4. (Top) Input images. (Bottom) Vessel centerlines (red) and boundaries (green) estimated by our technique.

TABLE I

RMS AND MEDIAN ERRORS, IN PIXELS, IN CENTERLINE LOCALIZATION FOR VESSELS IN 10 IMAGES.

	Thin Vessels	Thick Vessels	All Vessels
RMS	1.853	2.182	2.112
Median	1.000	1.000	1.000

TABLE II

MEAN AND MEDIAN ERRORS IN ESTIMATING THE WIDTHS (IN PIXELS) AND ORIENTATIONS (IN DEGREES) OF VESSELS IN 10 IMAGES.

		Thin Vessels	Thick Vessels	All Vessels
Width	Mean	1.461	3.320	2.850
	Median	1.089	2.430	2.023
Orientation	Mean	10.587	8.491	9.021
	Median	6.995	5.969	6.264

centerlines are in red, while the boundaries are in green. In addition to the steps described in Section II we have performed a simple check, inspired by [9], to eliminate false detections. For every detected centerline pixel, the corresponding boundary pixels (Equation 1) should lie on edges and the gradient direction at the boundary pixels should be close to the orientation at the centerline pixel. We eliminate a vessel segment if a majority of its pixels fail this test. This simple test eliminates several false positives, especially on the optic disk boundary. Note that our approach does not detect vessel bifurcations, since matched filters do not 'fire' at such intensity structures. Consequently, vessels are split up at bifurcations. We intend to address this splitting of vessels in future work.

For quantitative evaluation, we compared the estimated centerlines in 10 images with handmarked centerlines. The images are 700×700 pixels. Table I shows the root mean square (RMS) and median errors in localizing vessel centerlines for thin, thick, and all vessels. In our evaluation, vessel segments with widths less than 9 pixels are considered thin, while segments with widths between 9 and 33 pixels are considered thick. The low errors – $\sim$ 2 pixels – attest to our approach's accuracy. It should be noted that since the groundtruth was marked manually, errors of the order of a pixel are to be expected in the groundtruth as well.

To evaluate the accuracy of the estimated vessel properties,we randomly selected a large number of points on vessel centerlines in 10 images and had users mark the widths and orientations of the vessels at those points. These groundtruth vessel properties were then quantitatively compared to the vessel properties estimated by our algorithm, the results of which are also shown in Table II. We would like to point out that since boundaries of vessels subtly fade into the background retina, marking them is highly subjective. Marking vessel orientations is even more subjective especially if the

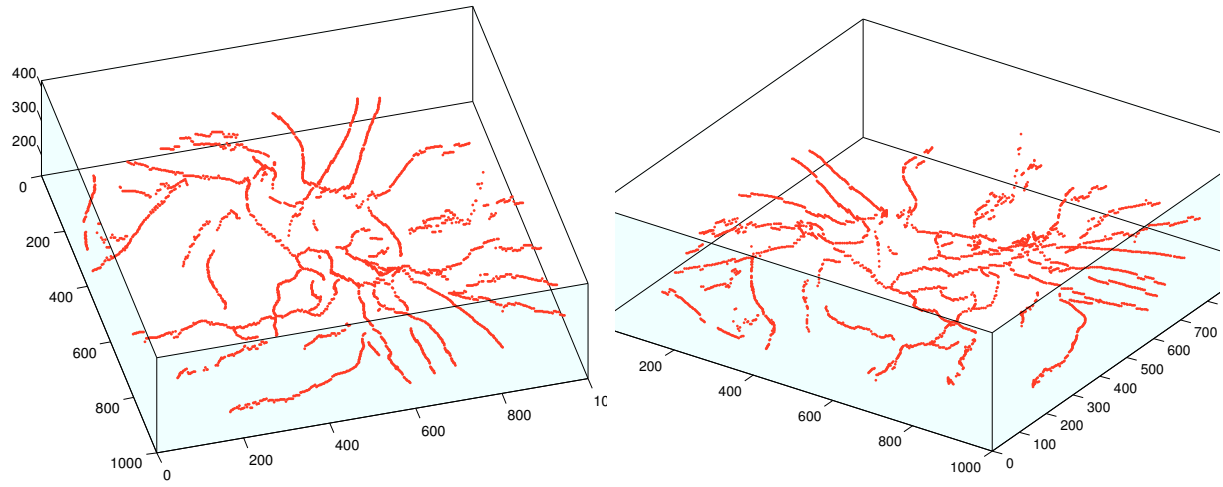

Fig. 5. Views of the 3D vessel network, obtained using stereo matching, of the eye shown in Fig. 1(b).

vessels are curving. Consequently, errors in the groundtruth for widths and orientations are expected.

IV. CONCLUSION

We present an automatic technique for localizing blood vessels in eye images with high accuracy. Our approach accounts for vessels with central reflex and also estimates the local width and orientation of vessels. Accurate centerlines enable us to correctly visualize vessel networks. Fig. 5 shows views of the 3D vessel network obtained by computing stereo disparities for the centerline pixels shown in Fig. 1(d), given a pair of eye images. For this we used normalized cross correlation matching with fixed windows. In future, we would like to use the estimated local vessel properties to adapt the widths and orientations of matching windows. Such an adaptive scheme should enable superior 3D reconstruction of vessels. Future work will also evaluate using the estimated local properties for diagnosing retinal vascular diseases like retinopathy of prematurity (ROP), which is characterized by dilation of vessels and increase in their tortuosity.

REFERENCES

[1] S. Aylward and E. Bullitt. Initialization, noise, singularities, and scale in height-ridge traversal for tubular object centerline extraction. *IEEE Transactions on Medical Imaging*, pages 61–75, 2002.

[2] S. Chaudhuri, S. Chatterjee, N. Katz, M. Nelson, and M. Goldbaum. Detection of blood vessels in retinal images using two-dimensional matched filters. *IEEE Transactions on Medical Imaging*, 8(3):263269, 1989.

[3] A. Frangi, W. Niessen, K. Vincken, and M. A. Viergever. Multiscale vessel enhancement filtering. *International Conference of Medical Image Computing and Computer-Assisted Intervention*, pages 130–137, 1998.

[4] T. Hastie, R. Tibshirani, and J. Friedman. *The Elements of Statistical Learning*. Springer, 2009.

[5] S. Kalitzin, J. Staal, B. ter Haar Romeny, and M. Viergever. A computational method for segmenting topological point-sets and application to image analysis. *IEEE PAMI*, 23(5):447–459, 2001.

[6] A. Mendonça and A. Campilho. Segmentation of Retinal Blood Vessels by Combining the Detection of Centerlines and Morphological Reconstruction. *IEEE Transactions on Medical Imaging*, 25(9), 2006.

[7] H. Narasimha-Iyer, V. Mahadevan, J. Beach, and B. Roysam. Improved Detection of the Central Reflex in Retinal Vessels Using a Generalized Dual Gaussian Model and Robust Hypothesis Testing. *IEEE Transactions on Information Technology in Biomedicine: A Publication of the IEEE Engineering in Medicine and Biology Society*, 12(3):406, 2008.

[8] N. Sang, Q. Tang, X. Liu, and W. Weng. Multiscale Centerline Extraction of Angiogram Vessels Using Gabor Filters. *Lecture Notes in Computer Science: Computational and Information Science*, 3314:570–575, 2005.

[9] M. Sofka and C. Stewart. Retinal vessel centerline extraction using multiscale matched filters, confidence and edge measures. *IEEE Transactions on Medical Imaging*, 25(12):1531–1546, 2006.

[10] K. Vermeer, F. Vos, H. Lemij, and A. Vossepoel. A model based method for retinal blood vessel detection. *Computers in Biology and Medicine*, 34:209–219, 2004.

[11] T. Zhu. Fourier cross-sectional profile for vessel detection on retinal images. *Computerized Medical Imaging and Graphics*, 34(3):203–212, 2010.